

to appear in Astronomical Journal

The kinematics of the warm gas in the interacting Hickson compact group of galaxies HCG 90

H. Plana and C. Mendes de Oliveira ¹

Instituto Astronômico e Geofísico (IAG), Av Miguel Stéfano 4200 CEP: 04301-904 São Paulo
Brazil

and

P. Amram and J. Boulesteix

IGRAP, Observatoire de Marseille, 2 Place Le Verrier, F-13248 Marseille Cedex 04, France

ABSTRACT

We present kinematic observations of H α emission for two early-type galaxies and one disk system, members of the Hickson compact group 90 (HCG 90) obtained with a scanning Fabry-Perot interferometer and samplings of 16 km s^{-1} and $1''$. Mapping of the gas kinematics was possible to $\sim 2 \text{ r}_{eff}$ for the disk galaxy N7174 and to $\sim 1.3 \text{ r}_{eff}$ and $\sim 1.7 \text{ r}_{eff}$ for the early-type galaxies N7176 and N7173 respectively. Evidence for ongoing interaction was found in the properties of the warm gas of the three galaxies, some of which do not have stellar counterparts.

The system H90bd (N7176-N7174) which was previously suspected to be an optical double may in reality be a system in interaction. In the region where the galaxies spatially overlap in projection (their continuum centers are only $25''$ apart), the gas profiles are separated in velocity space by $\sim 50\text{--}100 \text{ km s}^{-1}$. The gas component of the early-type galaxy is highly concentrated in the region closest to the irregular galaxy, where the interaction between the two galaxies may be taking place. The velocity fields of these galaxies are disturbed, most probably due to the ongoing interaction; they indicate that the galaxies are in pro-grade orbits, which is a favourable condition for merging.

H90c, morphologically classified as an elliptical galaxy, has a disk of ionized gas which rotates around an axis oriented 60° with respect to the stellar rotation axis. This is a strong evidence that the gas has an external origin. As is also the case for H90b, this galaxy may be a true S0 that was misclassified as an elliptical galaxy.

We suggest the following evolutionary scenario for the system. H90d is the warm gas reservoir of the group in process of fueling H90b with gas. H90c and d have

¹Present address: Universitaets-Sternwarte, Ludwig-Maximilians-Universitaet Scheinerstrasse 1, 81679 Muenchen, Germany.

experienced past interaction with gas exchange. The gas acquired by H90c has already settled and relaxed but the effects of the interaction can still be visible in the morphology of the two galaxies and their stellar kinematics. This process will possibly result in a major merger.

Subject headings: galaxies: elliptical and lenticular — galaxies: evolution — galaxies: formation — galaxies: individual (NGC 7173, NGC 7174, NGC 7176) — galaxies: interactions — galaxies: ISM — galaxies: kinematics and dynamics — instrumentation: interferometers

1. Introduction

Hickson compact groups of galaxies are small systems of three to seven galaxies with projected separations on the sky of a few galactic diameters and velocity dispersions comparable to the internal stellar motions of the group galaxies. Although several Hickson groups have a high projected galaxy density and seem to form a physical group, the hypothesis that a close system in projection is also compact in 3-D is only confirmed when the member galaxies are found to be in interaction with one another. If so, the low relative velocity dispersion of galaxies in the group as well as the small distances between them will favor the formation of merger remnants (Barnes 1989).

Several photometric and spectroscopic indicators of galaxy interactions have been identified in the literature such as shells, ripples, isophote twists, double nuclei, kinematically decoupled cores in ellipticals (Bertola et al. 1988) and disturbed rotational velocity curves of disks (Rubin et al. 1991). Other useful indicators of galaxy interactions can be found in the cold and warm gaseous component of a galaxy. Cold gas is very important in identifying late-type but not early-type interacting galaxies, since these are mostly devoid of HI (van Gorkom 1991, van Gorkom 1997). Warm gas, in contrast, is present in both early and late-type galaxies and can be used as a tracer of recent or on-going interactions. Although the warm gas component usually contributes only a small fraction of the total mass of a galaxy, it responds very quickly to gravitational perturbations and should therefore allow a detailed study of the recent history of interactions/accretions of the system.

We have begun a program to study the warm gas properties and kinematics of galaxies in a subsample of Hickson compact groups with the main aim of identifying interaction and merging signs among the member galaxies and in this way attempt to determine the evolutionary stage of the compact group. Paper I (Mendes de Oliveira et al. 1998) was dedicated to the compact group HCG 16, a system in an advanced evolutionary stage containing four late-type galaxies, where three of the members were shown to be merger remnants from the study of their gas properties.

The object of the present study is HCG90 (also called M59, N7171, LGG 450, Klemola 34), a

group at a distance of $33.15 h^{-1}$ Mpc (Faber et al. 1989, h is the dimensionless Hubble constant $H_0/100 \text{ km sec}^{-1} \text{ Mpc}^{-1}$) containing two late-type galaxies, NGC 7172 (H90a) and NGC 7174 (H90d), and two early-type galaxies, NGC 7176 (H90b) and NGC 7173 (H90c). This group was originally cataloged by Hickson (1982). The mean systemic velocity and velocity dispersion of the quartet were determined to be 2643 km s^{-1} and 100 km s^{-1} respectively (Hickson et al. 1992). The spectroscopy survey of a circular region with diameter $d = 1^\circ$ ($\sim 0.6 h^{-1}$ Mpc) centered on the group confirmed the result of Ramella et al. (1994) that H90 is a compact system surrounded by a loose group (de Carvalho et al 1997). Five new members were identified by this study. The velocity dispersion of this enlarged system of nine galaxies is 166 km s^{-1} . Yet more new members were identified when a larger area around HCG 90 was surveyed (1.5×1.5 degrees) by Zabludoff and Mulchaey (1998). A total of 16 galaxies were found at the redshift of the group, with a velocity dispersion of 190 km s^{-1} . A general trend of constant velocity dispersion with increasing radius of the group was detected for a combined sample of nine x-ray detected groups including HCG 90 suggesting that the groups may be embedded in a common dark matter halo (Zabludoff and Mulchaey 1998).

The four galaxies in the core of group HCG 90 are infrared emitters, detected both at 60 and $100 \mu\text{m}$ (Allam et al. 1996, for H90b and H90c only upper limits for the fluxes are available). Only H90a is a radio emitter in 6 and 20 cm (Menon 1995). Neutral hydrogen was detected for H90a and not for the other members of the group (Oosterloo & Iovino 1997). CO was detected in all galaxies (Boselli et al. 1996, Verdes Montenegro et al. 1998). The spectroscopic study of Coziol et al. (1997) showed that H90a and d have active cores. H90d is classified as an AGN and H90a is a Seyfert 2 galaxy. A halo of diffuse x-ray emission was detected around the group to a radius of $135 h^{-1} \text{ kpc}$ (Mulchaey and Zabludoff 1998). The emission is not centered on any galaxy of the group.

A study of the stellar kinematics of three of the member galaxies (H 90b, c and d) was done by Longo et al. 1994 (hereafter referred to as L94). Their study was based on spectra obtained using long-slit observations along two position angles of the galaxies (major axis and on one other position angle). Those data are used in Section 4.1 of this paper for a comparison with the properties of the gas kinematics of the galaxies.

In the present paper we present Fabry-Perot data of three galaxies of HCG 90: two early-type galaxies (H90b and c) and one late-type spiral galaxy (H90d). The observations and data reduction are presented in section 2. In section 3 we present a general description of each object with comments on the velocity fields (VFs), monochromatic maps and the velocity curves (VCs). The discussion is in section 4. It includes a comparison between the warm gas and the stellar kinematics of the galaxies.

2. Observations and data reduction

A two-hour exposure on galaxies H90b, c and d of HCG 90 has been obtained using the 3.6m ESO telescope in La Silla (Chile) on August 28th, 1995. The instrument CIGALE (CInématique des GALaxiEs, Boulesteix et al. 1983) attached to the Cassegrain focus was used. CIGALE is composed of a focal reducer (bringing the original f/8 focal ratio of the Cassegrain focus to f/2), a scanning Fabry-Perot, a narrow band interference filter and an Image Photon Counting System (IPCS) detector. The IPCS, with a time sampling of 1/50 s and zero readout noise makes it possible to scan the interferometer rapidly (typically 5 s per channel) avoiding sky transparency, airmass and seeing variation problems during the exposures. The basic principles of this instrument were described in Amram et al. (1991). The journal of the observations are given in Table 1. Table 2 lists the parameters for the three observed galaxies. The spatial and spectral sampling are $0.91''$ and 16 km s^{-1} respectively.

Reduction of the data cubes were performed using the CIGALE/ADHOC software (Boulesteix 1993). The data reduction procedure has been extensively described in Amram et al. (1996) and references therein.

Wavelength calibrations were obtained by scanning the narrow Ne 6599 Å line under the same conditions as the observations. The relative velocities with respect to the systemic velocity are very accurate, with an error of a fraction of a channel width ($< 3 \text{ km s}^{-1}$) over the whole field.

The signal measured along the scanning sequence was separated into two parts: (1) an almost constant level produced by the continuum light in a 10 Å passband around $\text{H}\alpha$ (continuum map), and (2) a varying part produced by the $\text{H}\alpha$ line (monochromatic map). The continuum level was taken to be the mean of the three faintest channels, to avoid channel noise effects. The monochromatic map was obtained by integrating the monochromatic profile in each pixel. The velocity sampling was 16 km s^{-1} . The monochromatic maps had one-pixel resolution in the center of the galaxies. Spectral profiles were binned in the outer parts (to 5×5 pixels) in order to increase the signal-to-noise ratio. When multiple components were visually present, the lines were decomposed into multiple Gaussian components. OH night sky lines passing through the filters were subtracted by determining the shapes and intensities of the lines away from the galaxies (Laval et al. 1987).

A rough flux calibration of the monochromatic images was attempted by adjusting the flux levels to those of the calibrated image of the Cartwheel galaxy, obtained in the same run (see details of how the Cartwheel galaxy image was calibrated in Amram et al. 1998). $\text{H}\alpha$ profiles for the HCG 90 galaxies were measured to a minimum flux density between $0.2 \times 10^{-17} \text{ erg s}^{-1} \text{ cm}^{-2} \text{ arcsec}^{-2}$ and $3 \times 10^{-17} \text{ erg s}^{-1} \text{ cm}^{-2} \text{ arcsec}^{-2}$ (corresponding to a S/N between three and five).

3. Results

Fig. 1 presents a contour plot of the continuum map of the H90 group. The total field of view is $3.5' \times 3.5'$. The continuum map was made using a spatial square smoothing box of 3×3 pixels. Figs. 2 to 8 show the monochromatic images, the velocity fields (VFs) of $H\alpha$, the velocity curves (VCs) and a plot of the variation of the kinematic PA with radius. The line-of-sight velocities plotted have not been adjusted by the cosmological correction ($1 + z$).

We can directly compare the line-of-sight velocity curves of the three galaxies studied here, since by chance their inclinations are very similar ($\sim 55^\circ$). Therefore, no deprojection of the velocities was done, for the plots in Figs. 3, 6 and 8, although the maximum velocities listed in Table 2 do include the deprojection as do also the determinations of the masses.

Detailed discussion on the method used to obtain the systemic velocity, center, position angle (PA) of the major axis and inclination of the galaxy are given in Amram et al. (1996).

3.1. H90c (NGC 7173)

H90c has been classified as an E0 galaxy by Hickson (1993) and as an E+pec galaxy in the RC3 catalogue. Its low ellipticity ($\epsilon = 0.26$) makes it difficult to determine the PA of its major axis. In the inner part (out to $10''$) it is $\sim 60^\circ$ and in the outskirts of the galaxy it reaches 130° (all PA measurements are made from north to east).

Figs. 2a and 2b present respectively the monochromatic image and the velocity field. Emission is measured out to a radius of $\sim 25''$, which represents $1.7 r_{eff}$ or $4 h^{-1}$ kpc (using r_{eff} given by L94). We can see, on Fig.2a, a small excess of gas in a region located to the north at $6.6''$ from the center.

The velocity field for H90c presents a peculiarity in the SE, where some of the iso-velocities with signal-to-noise $S/N \sim 3$ (velocities 2800 km s^{-1} and 2820 km s^{-1}) are inconsistent with the rest of the map. In the center of the galaxy, the S/N of the data is typically 30.

The variation of the PA of the kinematic major axis with radius for H90c (not presented here) is small. From the center to $22''$ the PA varies continuously from 20° to 40° . The line-of-sight velocity diagram (hereafter referred to as VC for velocity curve) presented in Fig. 3a, has been built with a $PA=40^\circ$. It shows a maximum velocity amplitude of $\pm 70 \text{ km s}^{-1}$, which is significantly lower than that for H90b and H90d. The mean PA of the major axis given by the gas kinematics, $40^\circ \pm 5^\circ$, differs by 60° from the corresponding stellar kinematic major axis of 100° (as given by L94; see also Section 4.1).

The NE side of the velocity curve of H90c is not as flat as the SW side. This may be due to a local starburst in the NE of the galaxy, which induces proper motions (see Fig. 2).

The center of the galaxy as measured from the continuum image coincides with the monochromatic center within the seeing disk ($\sim 1''$). The kinematic center, however, is situated $2''$ to the west of the other two centers. The gas systemic velocity, as measured from the VF, is $2785 \pm 15 \text{ km s}^{-1}$. Hickson (1989) and de Carvalho et al. (1997) found systemic velocities of $2696 \pm 24 \text{ km s}^{-1}$ and $2497 \pm 12 \text{ km s}^{-1}$ respectively, from measurements using absorption lines. The central velocity dispersion of the galaxy, as measured by the full width of half maximum (FWHM) of the gas profile is $80 \text{ km s}^{-1} \pm 15$ (after deconvolution by the instrumental profile of FWHM $\sim 35 \text{ km s}^{-1}$). This central value decreases to $63 \text{ km s}^{-1} \pm 16$ towards the external regions.

The integrated flux calculated for the total gas extension is $F(\text{H}\alpha) = 1.45 \pm 0.12 \times 10^{-14} \text{ erg s}^{-1} \text{ cm}^{-2}$. Using the formula given by Osterbrock (1974) with an electronic density of 1000 cm^{-3} , we have derived a mass of ionized gas of $M_{\text{HII}} = 0.45 \pm 0.04 \times 10^4 M_{\odot}$. This may, however, be an upper limit on the gas mass, since the value we take for the electronic density is also an upper limit.

We used the formula from Lequeux (1983) (with $f=1$) to determine the total mass of the galaxy. We have obtained $M_{\text{tot}} = 0.48 \times 10^{10} \pm 0.13 M_{\odot}$ (see Table 2).

3.2. H90b (NGC 7176)

H90b has been classified as an E0 galaxy by Hickson (1993) and as an E+pec galaxy in the RC3 catalogue (De Vaucouleurs et al. 1991). As for HCG 90C, the round shape of this object is a problem to determine the PA of the major axis. Mendes de Oliveira (1992) reported a value of $55^{\circ} \pm 5^{\circ}$ from the analysis of an R image of the galaxy which is consistent with the values of $53^{\circ} \pm 10^{\circ}$ (see Fig. 1) and $55^{\circ} \pm 10$ determined from the continuum and monochromatic images respectively.

In Figs. 4a and 4b we show the monochromatic and velocity maps for the ionized gas component of H90b. The warm gas in H90b can be measured out to a radius of $\sim 20''$ which represents $1.3 r_{\text{eff}}$ or $3.2 h^{-1} \text{ kpc}$ (using r_{eff} given by L94). The iso-velocities of the VF are fairly regular in the east side of the galaxy. In the SW direction, however, the situation is much more confusing. The distribution of the ionized gas is very clumpy. For this reason it is difficult to determine its center. An excess of gas is observed in the SW part of the galaxy, towards H90d.

Fig. 5 shows the variation of the PA of the major axis with radius, derived from the VF. The kinematic PA of the major axis raises continuously from $\sim 0^{\circ}$ to 100° at a $17''$ -radius. The mean PA of the major axis given by the gas kinematics, $60^{\circ} \pm 5^{\circ}$, differs by 70° from the corresponding stellar kinematic major axis of $\sim 130^{\circ}$ (as given by L94; see also Section 4.1).

We find that the FWHM of the emission-line profiles of H90b are slightly lower than those for H90c. We find a mean FWHM of $\sim 60 \pm 10 \text{ km s}^{-1}$ in the center (after correction for an instrumental profile of FWHM $\sim 35 \text{ km s}^{-1}$). This value decreases with distance to the center to

$47 \pm 10 \text{ km s}^{-1}$ at a $15''$ -radius.

Fig. 6 presents the VC derived from the velocity field of H90b with a $\text{PA}=60^\circ$, our best determination of the kinematic major axis of the galaxy. This curve was built using the kinematic center (situated $3.3''$ to the NE of the continuum center) and its corresponding velocity of $2540 \pm 12 \text{ km s}^{-1}$. As a comparison, Hickson et al. (1992) and de Carvalho et al. (1997) give systemic velocities for H90b of $2525 \pm 29 \text{ km s}^{-1}$ and $2511 \pm 14 \text{ km s}^{-1}$ respectively, measured from absorption lines. H90b has an asymmetric VC, rare among isolated galaxies. The maximum velocity observed is $+75 \text{ km s}^{-1}$ and the minimum is -110 km s^{-1} .

The total integrated $\text{H}\alpha$ flux inside a $18''$ -radius is $7.8 \pm 0.15 \times 10^{-15} \text{ erg s}^{-1} \text{ cm}^{-2}$, which gives a gas mass of $M_{\text{HII}}=0.24 \pm 0.04 \times 10^4 M_\odot$ (assuming an electronic density of 1000 cm^{-3}). This gives an upper limit for the warm gas mass.

The total mass of the galaxy, obtained using the formula of Lequeux (1983), was found to be $M_{\text{tot}}=0.82 \times 10^{10} \pm 0.25 M_\odot$ (Table 2).

3.3. H90d (NGC 7174)

This object has been classified as an Irregular galaxy by Hickson (1989) and as an early-type spiral by the RC3 catalogue (de Vaucouleurs et al. 1991). The PA of its major axis, as derived from the continuum image is $85^\circ \pm 10^\circ$ and $75^\circ \pm 5^\circ$ from the monochromatic image.

Figs. 7a and 7b present respectively the monochromatic image and the velocity field. Emission is measured out to a radius of $\sim 15''$. Fig. 7a shows a gas extension in the east side of the galaxy, towards H90b. Fig. 7b shows disturbed iso-velocities in the NE and SW direction.

The monochromatic center coincides with the center of the continuum image (within the seeing disk). Both are, however, separated from the kinematic center by approximately $3''$ (Fig. 7b). Our best determination of the mean PA of the major-axis is $75^\circ \pm 5^\circ$ (as measured from the overall geometry of the kinematic map).

The PA of the monochromatic image does not change significantly with radius while the PA of the kinematic major axis does (see Fig. 5). The variation of the PA of the kinematic major axis for H90d shown in Fig. 5 suggests the presence of a strong warp.

The systemic velocity is determined from the VF to be $2635 \pm 15 \text{ km s}^{-1}$, similar to the systemic velocity given by de Carvalho et al. (1997) of $v_{\text{sys}}=2659 \pm 9 \text{ km s}^{-1}$, also determined from emission lines.

The VC shown in Fig. 6 was derived from the VF, along the kinematic major axis, $\text{PA}=75^\circ$. It reaches a maximum velocity of $+200 \text{ km s}^{-1}$ at $15''$ from the nucleus, in the SW side. In the NE side it reaches a minimum of -150 km s^{-1} at a $28''$ -radius. The motion is not axisymmetric. On the SW side of the curve, the VC is perturbed as displayed by two of the iso-velocities present

in that region. A possible explanation is the presence of a dust lane which affects the VF.

The velocity dispersion at the position of the kinematic and continuum centers are respectively $110 \pm 10 \text{ km s}^{-1}$ and $120 \pm 10 \text{ km s}^{-1}$ (after correction for an instrumental profile of FWHM $\sim 35 \text{ km s}^{-1}$. Further to the east it decreases to $90 \pm \text{km s}^{-1}$.

The total gas flux derived within a $16''$ -radius is $F(\text{H}\alpha) = 2.39 \pm 0.12 \times 10^{-14} \text{ erg s}^{-1} \text{ cm}^{-2}$, which gives an upper limit on the gas mass of $M_{\text{HII}} = 1.0 \pm 0.04 \times 10^4 M_{\odot}$.

We obtain a total mass for this galaxy of $M_{\text{tot}} = 2.4 \times 10^{10} \pm 0.2 M_{\odot}$ (see Table 2).

4. General discussion of the results

4.1. Comparison with the Stellar Kinematics of the Galaxies

L94 have carried out a study of the stellar kinematics of the HCG 90 galaxy members. They concluded that H90c and H90d are in interaction and H90b and H90d are not. This last point is contrary to our results.

We give details of the comparison between the stellar and gaseous kinematics for each of the galaxies below.

- H90c:

L94 presented stellar velocity curves for H90c along slits placed at $\text{PA}=130^\circ$ and $\text{PA}=147^\circ$. We present here a comparison at only one of these position angles, since the kinematics of the gas does not change significantly between these two positions.

Fig. 3b presents (with crosses) the VC derived from the $\text{H}\alpha$ kinematics, along a $\text{PA}=130^\circ$, which coincides with the gas kinematic minor axis of the galaxy. We would expect to find a flat curve, if no motion was present along the minor axis. We detect, however, a small velocity gradient due to: 1) two inconsistent isovelocities in the SE part of the VF (see Fig. 2b) which produces positive velocities on the VC ($+50 \text{ km s}^{-1}$ at $13''$) and 2) on the NW side, the cross section at $\text{PA}=130^\circ$ includes two twisted iso-velocities which produces negative velocities on the VC (-50 km s^{-1} at $18''$). These features are produced by iso-velocities with $\text{S/N} \sim 3$ and 8 respectively.

We have overplotted in Fig. 3b the stellar VC (from L94, his Fig. 3a) determined at the same PA of 130° . The shapes of the gas and stellar curves are very different. For the gas kinematics we do not see the “U shape” described by the stellar kinematics. Another striking difference is the lack of a flat portion in the velocity curve along the major axis of the stellar component and the presence of an irregular velocity gradient that goes up to 300 km s^{-1} with no regular motion, contrary to what is seen at a cut along the kinematic major axis of the gas component (shown in Fig. 3a). According to L94 the stellar major axis of the galaxy

may be at 100° (corresponding to a rotating axis of 10°). Therefore, the cut at $\text{PA}=130^\circ$ is close to the major axis defined by the stellar kinematics and should show a large velocity gradient, as it indeed does.

The stellar and gaseous motions are strongly decoupled (by about $100^\circ-40^\circ=60^\circ$). The kinematics of the gaseous component is more well behaved than that of the stellar component. This is evidence that this early-type galaxy contains a gas disk with well ordered circular motion.

- H90b+d:

These two galaxies have strongly overlapping isophotes. Their continuum centers are separated by only $25''$ ($4 \text{ h}^{-1} \text{ kpc}$).

The non-interaction between H90b and H90d claimed by L94 was based on the following evidence: 1) no disturbances were found in the internal stellar velocity curves of the two galaxies along an axis which joins their centers ($\text{PA}=68^\circ$) and 2) the parabolic velocity calculated for these two galaxies is twice their systemic velocity difference. Point (1) is discussed below and point (2) is discussed in the next section.

The stellar velocity curve obtained along the line joining the centers of H90b and H90d ($\text{PA}=68^\circ$) was given by L94 (their Fig. 7a) and it can be directly compared to our Fig. 8. The gas velocity curve shown in Fig. 8 was obtained by doing a cross-section of the gas velocity maps of H90b and H90d at $\text{PA}=68^\circ$ and using the continuum center and the systemic velocity of H90b as a reference point (position 0,0 in Fig. 8), in order to be consistent with L94. Since it was not specified in L94's paper which systemic velocity was used to draw their Fig. 7a, we will make a comparison of the shape and extension of the curves only, not of the absolute values for the maximum velocities.

The first obvious difference when comparing the gas and stellar curves is the contrast between the *continuous stellar* rotation curves of H90b and H90d with the *break* in velocity space between the two corresponding *gaseous* components. This may occur, at least in part, because our observations are made at higher resolution than L94's observations.

We also see a strong discrepancy between the shape of the gaseous and stellar components for H90b (around position 0,0 in Fig. 8). The stellar component is almost flat while the gas curve displays a large velocity gradient. This is easily understood if we remember that the position angle $\text{PA}=68^\circ$, along which the measurements are plotted in Fig. 8, is very close to the kinematic major axis of the gas component of H90b ($\text{PA}=60^\circ$, see Table 2) but almost perpendicular to the kinematic major axis of the stellar component ($\text{PA} = 130^\circ$, see L94). Therefore we would expect the velocity curves for the two components of H90b to have very different shapes, as is indeed observed.

The shapes of the stellar and gaseous velocity curves of H90d, in contrast, are in general agreement (in the region where a comparison is possible, i.e., to the SW side of the galaxy).

This was expected given that the major axes of the gas and stellar components of H90d have the same orientation (PA \sim 75°).

Further comparison of the gaseous and stellar curves show that the stellar measurements do not go as far to the NE as the gas velocity curve does. The opposite is true for the SW region. The more extended stellar velocity curve on this side may be due to a light extension detected by L94 but not seen in the ionized gas (perhaps because of too low S/N of our data in that region).

A plot of our data for H90b along a PA=130° (not shown here) confirms that this is indeed the minor axis of the gas kinematic disk (the curve is flat). This contrasts with the curve drawn at the same PA (in Fig. 3a of L94) for the stellar component, which displays a velocity gradient. It is clear from the comparison described above that the kinematics of the stellar and gaseous components of H90b are strongly decoupled (by about 130°–60°=70°).

In order to convince the reader that the gaseous velocity profiles of H90b+d are separated and can be measured in the region of overlap we plot in Fig. 9 part of the 2-D H α map. The upper pannel indicates with a bold square the region within which the H α profiles are shown in the lower pannels. The lower left and right pannels show respectively the measured profiles and the best gaussian fits to the data (of FWHM = 63 km s⁻¹). Each small square in the lower pannels correspond to a 0.91'' \times 0.91'' – pixel and a velocity interval of 380 km s⁻¹. We can clearly measure both components of H90b and H90d in the overlapping region.

- Parabolic velocities

L94 argued that the system H90b+d is not in interaction. One of the reasons presented was the fact that the parabolic velocity is much larger than the difference between the two systemic velocities. We did the same calculation using the gas parameters (the gas central velocity and the total mass determined from the gas kinematics and the virial theorem) and we find as parabolic velocities $V_{para}=130 \pm 45$ km s⁻¹ and $V_{para}=230 \pm 55$ km s⁻¹ for the systems H90c+d and H90b+d respectively. This can be compared with the central gas systemic velocity differences of 150 ± 30 kms⁻¹ and 95 ± 30 km s⁻¹ respectively. Errors bars are large, and therefore the discrepancy between the parabolic velocities and velocity differences may be not significant.

4.2. Misclassification of two members

H90b and H90c have been previously classified as elliptical galaxies. Our kinematic study of the gas component, however, show that these two objects may be S0 galaxies.

Combining the gas and stellar kinematic data, we conclude that H90b and H90c may be S0 galaxies. According to L94, the ratio V/σ of H90c, as measured from the stellar component, is 0.7 for an apparent ellipticity of 0.26. This places H90c in the V/σ *vs.* ellipticity diagram of Davies et al. (1987) in the domain of the rotationally supported objects. Our gas study leads to the same

conclusion, with $V/\sigma = 0.87$ for an apparent ellipticity of 0.1. Likewise, for H90b, the stellar V/σ is 0.6, for an apparent ellipticity of 0.28, and for the gas component the V/σ is 1.6 for an apparent ellipticity of 0.6. Therefore, both H90b and H90c may be rotationally supported objects.

We conclude from the position of H90b and H90c in the V/σ *vs.* ellipticity diagram that these are misclassified S0 galaxies.

4.3. Ionized gas mass to K-band luminosity ratio

Fig. 10 presents the ratio of mass of HII gas to K band luminosity as a function of radius from the center of the galaxy for galaxies H90b, c and d. The HII gas masses have been derived from the calibrated monochromatic images and transformed into mass densities in $M_{\odot} \text{ pc}^{-2}$. The K band luminosity profiles come from unpublished photometry by Mendes de Oliveira, transformed into surface density in $L_{\odot} \text{ pc}^{-2}$. The absolute scale for the K photometry is not accurate but the relative differences in the shapes and intensities of the curves in Fig. 11 are not affected by this uncertainty given that the zero point of the K photometry is identical for the three galaxies. Tables 3, 4 and 5 give details of the plots shown in Fig. 10.

The two early-type galaxies, H90b and H90c, present a lower mean M_{HII}/L_K ratio than H90d. The M_{HII}/L_K of H90c and H90d raise regularly with approximately the same slope. The slope of the curve of H90b is, however, very different from those for the two other galaxies. For H90b the M_{HII}/L_K increases rapidly from $-7.0 M_{\odot} / L_{\odot}$ at a radius of $4''$ to $-5.75 M_{\odot} / L_{\odot}$ at $15''$ from the center. After that it decreases slowly. The rapid increase corresponds to the gas excess present in the monochromatic map of H90b (see Fig. 4a). Between radii $15''$ and $20''$, the M_{HII}/L_K ratio increases for H90d while it decreases for H90b. An analysis made by Hibbard et al. (1995) of the HI content of several merger remnants showed that an increase of the M_{HI}/L_K in the outer parts of an interacting system is a strong signature of a late-stage encounter. We cannot be as affirmative here, mainly due to the extension of the gas which is very small compared to that for the HI gas. What we can say, however, is that we detect a significant difference in the behaviour of the M_{HII}/L_K *vs.* radius curve for H90b, as compared to those for H90c and H90d.

In a scenario where H90d is considered as a gas reservoir and H90b is the “recipient”, it seems plausible to find a higher amount of gas for H90d and a higher M_{HII}/L_K ratio in the extreme part of H90b, where the gas exchange is taking place.

4.4. On-going interaction signatures

- Insights from the study of the kinematics and gas content

The values listed in Table 2 show that the total ionized gas mass in H90d is four times higher than that for H90b and twice as high as that of H90c. The values found for the

two early-type galaxies, however, even if small, are consistent with previous studies of the interstellar medium (ISM) of elliptical and lenticular galaxies in other environments (Goudfrooij et al. 1994, Macchetto et al. 1996). What is anomalous in the early-type galaxies H90b and H90c is not their gas content but their gas kinematics, as summarized below.

- H90c:

The strong decoupling between the warm gas and the stellar major axes for this galaxy and the contrast between the well behaved kinematics of the gas and the ‘U-shape’ kinematics of the stars along its kinematic major axes suggest that the gas disk of H90c is of external origin. It may be the result of an interaction. The gas is relaxed while the stars still feel the effects of a recent interaction.

- H90b+d:

The VFs and the monochromatic maps of this system strongly suggest that there is an interaction in progress taking place between these two galaxies. The VFs of the two galaxies are twisted and the VCs show non-axisymmetric motions. The monochromatic maps show evidence that there is a gas bridge between these two galaxies: there is an excess of ionized gas in the SW side of H90b, towards H90d, and the gas distribution is non-axisymmetric with an extension to the NE side of H90d, in the direction of H90b.

L94 concluded that there is no strong observational evidence for an interaction in progress between H90b and d from the stellar kinematics. This difference between the kinematics of the gas and of the stars can arise, for an example, if the gas component responds more quickly to gravitational perturbations than the stellar component. In this case the gas kinematics may show evidences of interaction that do not have counterparts in the stellar kinematics.

The hypothesis that H90b+d form an interacting system is enforced by the observation that in binary galaxies the interaction is more efficient when the encounter is prograde (Alladin & Narasimhan 1982), which is the case for this system.

- Insights from other ISM phases

Other components of the ISM of the galaxy members can help determining the evolutionary stage of the compact group HCG 90.

Several studies show that HCG 90 has diffuse X-ray emission (Ponman et al. 1996, Mulchaey & Zabludoff 1998). The emission is not centered on any group member, suggesting that HCG 90 may be a young, dynamically evolving group.

H90a is not included in this study but HI observations for this galaxy are available by Oosterloo and Iovino (1997). Located at $8'$ or $77 \text{ h}^{-1} \text{ kpc}$ to the north of the other three members, the velocity difference between H90a and the rest of the group is only 100 km s^{-1} . The morphology of the HI emission is very disturbed, showing an extension in the

direction of the remaining group members (mainly to HCG 90C). Oosterloo and Iovino (1997) concluded that the HI morphology for this galaxy suggests a strong tidal interaction with the other group members.

CO emission has been detected in HCG 90 by Verdes-Montenegro et al. (1998) mainly centered on H90d. However Huchtmeier & Tammann (1992) show, from smaller beam data, that H90b also displays significant CO emission. The case of H90c is still not resolved. Verdes-Montenegro et al. (1998) indicate that this member presents only marginal CO emission, but they suggest that observations with a smaller beam may be able to confirm their detection.

4.5. Possible evolutionary scenario

We show in this paper several pieces of evidence that HCG 90 is a dynamically evolving group. The three galaxies are in interaction and will possibly merge into one single object.

We suggest the following scenario: H90d is the warm gas reservoir of the group. H90c and d have experimented a past interaction with gas exchange. The gas acquired by H90c has already settled and relaxed (as suggested by the well behaved shape of the gas velocity curve of H90c) but the effects of the interaction can still be visible in the morphology of the two galaxies and their stellar kinematics (L94). On the other hand, H90d is now in the process of fueling H90b with gas, a process that will possibly result in a major merger.

Our observations provide important constraints for the modelling of the kinematics of merging group galaxies.

The authors thank Chantal Balkowski for initializing the project and Jean-Luc Gach for mounting the instrument on the telescope and helping during the observations. P. Amram and J. Boulesteix thank the department of Astronomy at the IAG in São Paulo for the hospitality during their visit, in connection with this project. H. Plana acknowledges the financial support of the Brazilian FAPESP, under contract 96/06722-0. C. Mendes de Oliveira acknowledges the financial support from the Alexander von Humboldt foundation.

Table 1. Journal of Perot-Fabry observations

Compact Group of Galaxies Hickson 90		
Observations	Telescope	ESO 3.6m
	Equipment	CIGALE @ Cassegrain focus
	Date	August, 28th 1995
	Seeing	$\sim 1.2''$
Interference Filter	Central Wavelength	6624 \AA^1
	FWHM	10 \AA^2
	Transmission	0.6^1
Calibration	Neon Comparison light	$\lambda 6598.95 \text{ \AA}$
Perot–Fabry	Interference Order	796 @ 6562.78 \AA
	Free Spectral Range at $H\alpha$	380 km s^{-1}
	Finesse at $H\alpha$	12
	Spectral resolution at $H\alpha$	18750 at the sample step
Sampling	Number of Scanning Steps	24
	Sampling Step	0.35 \AA (16 km s^{-1})
	Total Field	$230'' \times 230''$ ($256 \times 256 \text{ px}^2$)
	Pixel Size	$0.91''$
Exposures times	Total exposure	2 hours
	Elementary scanning exposure time	5 s per channel
	Total exposure time per channel	300 s

¹For a mean beam of $2.7''$

²For a mean beam inclination of $2.7''$

Table 2. Physical Parameters of the Galaxies

Name	H90b	H90c	H90d
Other names	NGC 7176	NGC 7173	NGC 7174
α (1950) ¹	21 ^h 59 ^m 14.1 ^s	21 ^h 59 ^m 08.8 ^s	21 ^h 59 ^m 11.6 ^s
δ (1950) ¹	−32°11′36.4″	−32°11′30.4″	−32°11′26.3″
Morphological type (Hickson/RC3) ¹	E0/E+pec	E0/E+pec	Im/Sab
B_{TC} ¹	12.57	12.73	12.81
Systemic heliocentric velocity/ ¹ (km s ^{−1})	2525 ± 29	2696 ± 24	2778 ± 29
Gas central velocity/ ⁷ (km s ^{−1})	2540 ± 12	2785 ± 15	2635 ± 15
D(Mpc) ²	33.15	33.15	33.15
F(H α)10 ^{−14} erg s ^{−1} cm ^{−2} / ³	0.78 ± 0.15	1.45 ± 0.12	2.39 ± 0.12
Log L(H α) erg s ^{−1}	37.85 ± 0.20	38.2 ± 0.02	38.41 ± 0.05
M _{HII} ($\times 10^4$ M $_{\odot}$)	0.24 ± 0.04	0.45 ± 0.04	1.0 ± 0.04
Vrot _{max} (km s ^{−1})/ ⁴	122 ± 12	85 ± 12	220 ± 18
R _{max} (kpc)/ ⁵	2.40 ± 0.25	2.90 ± 0.25	2.20 ± 0.25
M _{tot} ($\times 10^{10}$ M $_{\odot}$)/ ⁶	0.82 ± 0.25	0.48 ± 0.13	2.4 ± 0.2
Major axis (gas kinematics)/ ⁷	60° ± 10	40° ± 5	75° ± 10
Major axis (stellar kinematics)/ ⁸	130°	100°	68°/74°
Major axis (H α image)/ ³	55° ± 10	51° ± 20	85° ± 5
Inclination of the gaseous disk ⁷	54° ± 3	55° ± 3	55° ± 5
FWHM of central profiles (km s ^{−1})	60 ± 16	80 ± 15	110 ± 8

References. — ¹ Hickson (1993); ² from Faber et al. (1989); ³ from calibrated monochromatic maps; ⁴ maximum rotation velocities (corrected for the gas-disk inclination); ⁵ radius at maximum velocity, using distance for the group from Faber et al. 1989; ⁶ total mass of the galaxy, determined using Lequeux’s (1983) formulae (with f=1.); ⁷ derived from the gas velocity map; ⁸ from L94

Table 3. H90b surface brightness and surface density.

Radius ¹ "	K ² mag/' ²	Log[$\sigma(K)$] ³ $L_{\odot}.pc^{-2}$	Log[$\sigma(HII)$] ⁴ $M_{\odot}.pc^{-2}$	Log[$\frac{\sigma(HII)}{\sigma(K)}$] ⁵ M_{\odot}/L_{\odot}
4.19	17.77	3.626	-3.310	-6.936
4.82	18.00	3.533	-3.319	-6.852
5.37	18.23	3.442	-3.384	-6.826
7.83	18.94	3.157	-3.394	-6.551
15.02	20.34	2.600	-3.102	-5.702
15.47	20.43	2.562	-3.102	-5.664
16.38	20.53	2.521	-3.132	-5.653
16.47	20.53	2.521	-3.136	-5.657
16.74	20.59	2.500	-3.201	-5.701
17.29	20.65	2.475	-3.250	-5.725
17.47	20.70	2.454	-3.272	-5.726
18.20	20.78	2.422	-3.396	-5.818
18.93	20.90	2.376	-3.425	-5.801
19.47	20.99	2.340	-3.486	-5.826
20.38	21.11	2.289	-3.543	-5.832

References. — ¹ Radius from the center in arcsec;

² Surface brightness in Mag/'²;

³ Logarithm of light surface density in L_{\odot}/pc^2 ;

⁴ Logarithm of gas surface density in M_{\odot}/pc^2 ;

⁵ Logarithm of gas mass to K bandluminosity ratio in M_{\odot}/L_{\odot} .

Table 4. H90c surface brightness and surface density

Radius ¹ "	K ² mag/' ²	Log[$\sigma(K)$] ³ $L_{\odot}.pc^{-2}$	Log[$\sigma(HII)$] ⁴ $M_{\odot}.pc^{-2}$	Log[$\frac{\sigma(HII)}{\sigma(K)}$] ⁵ M_{\odot}/L_{\odot}
2.57	17.15	3.825	-3.004	-6.829
2.81	17.36	3.792	-3.024	-6.816
3.21	17.55	3.716	-3.054	-6.770
3.37	17.63	3.681	-3.067	-6.748
3.60	17.75	3.636	-3.085	-6.721
3.81	17.83	3.602	-3.103	-6.705
4.11	17.91	3.571	-3.129	-6.700
4.54	18.08	3.504	-3.165	-6.669
5.24	18.39	3.376	-3.220	-6.596
5.81	18.55	3.314	-3.261	-6.575
6.45	18.77	3.225	-3.307	-6.532
7.67	19.09	3.097	-3.388	-6.485
10.73	19.86	2.792	-3.545	-6.337
15.25	20.79	2.417	-3.711	-6.128
19.98	21.69	2.056	-3.86	-5.916

References. — ¹ Radius from the center in arcsec;

² Surface brightness in Mag/'²;

³ Logarithm of light surface density in L_{\odot}/pc^2 ;

⁴ Logarithm of gas surface density in M_{\odot}/pc^2 ;

⁵ Logarithm of gas mass to K band luminosity ratio in M_{\odot}/L_{\odot} .

Table 5. H90d surface brightness and surface density

Radius ¹ "	K ² mag/' ²	Log[$\sigma(K)$] ³ $L_{\odot}.pc^{-2}$	Log[$\sigma(HII)$] ⁴ $M_{\odot}.pc^{-2}$	Log[$\frac{\sigma(HII)}{\sigma(K)}$] ⁵ M_{\odot}/L_{\odot}
1.82	17.64	3.680	-2.517	-6.192
2.00	17.69	3.660	-2.522	-6.182
2.18	17.74	3.640	-2.523	-6.163
2.37	17.75	3.635	-2.553	-6.188
2.55	17.84	3.600	-2.563	-6.163
2.82	17.78	3.624	-2.579	-6.203
3.09	17.82	3.607	-2.603	-6.210
3.37	17.90	3.576	-2.627	-6.203
9.65	18.94	3.159	-2.674	-5.833
14.38	19.47	2.947	-2.728	-5.675
15.11	19.55	2.914	-2.776	-5.690
15.83	19.69	2.860	-2.805	-5.665
19.66	20.66	2.472	-2.866	-5.338
20.84	20.82	2.407	-2.923	-5.330
21.29	20.89	2.380	-2.996	-5.376

References. — ¹ Radius from the center in arcsec;

² Surface brightness in Mag/'²;

³ Logarithm of light surface density in L_{\odot}/pc^2 ;

⁴ Logarithm of gas surface density in M_{\odot}/pc^2 ;

⁵ Logarithm of gas mass to K band luminosity ratio in M_{\odot}/L_{\odot} .

REFERENCES

- Alladin S.M., Narasimhan K.S.V.S., 1982, Physical Reports (Review Section of Physics Letters) 92, No6 p339
- Allam S., Assendorp R., Longo G., Braun M., Richter G., 1996 A&AS, 117, 39
- Amram P., Boulesteix J., Georgelin Y.P., Georgelin Y.M., Laval A., le Coarer E., Marcelin M., 1991, "The Messenger" (ESO), 64, 44
- Amram P., Balkowski C., Boulesteix J., Cayatte V., Marcelin M., Sullivan W. 1996, A&A, 310, 737
- Amram P., Mendes de Oliveira C., Boulesteix J., Balkowski C., 1998, A&A, 330, 881
- Barnes J., 1989, Nature, 338, 123
- Bertola F., Buson M., Zeilinger W., 1988, Nature 335, 20
- Boselli A., Mendes de Oliveira C., Balkowski C., Cayatte V., Casoli F., 1996, A&A, 314, 738
- Boulesteix J., 1993, "ADHOC reference manual", Publications de l'Observatoire de Marseille
- Coziol R., Ribeiro A.L.B., de Carvalho R.R., Capelato H.V., 1997, ApJ, 493, 563
- Davies R.L., 1987, in IAU Symposium 127: Structure and Dynamics of Elliptical Galaxies, ed. P.T. de Zeeuw (Dordrecht: Reidel), p. 63
- de Carvalho R., Ribeiro A., Capelato H.V., Zepf S., 1997, ApJ Suppl 110, 1
- de Vaucouleurs A., de Vaucouleurs G., Corwin J.R., Buta R., Paturel G., Fouque P. 1991, 3rd Reference Catalog of Bright Galaxies
- Faber S., Wegner G., Burstein D., Davies R., Dressler A., Lynden-Bell D., Terlevich R., 1989, ApJ Suppl. 69, 763
- Goudfrooij P., Hansen L., Jorgensen H.E., Norgaard-Nielsen H.U., 1994, A&AS, 105, 341
- Hibbard J.E., van Gorkom J.H., 1996, AJ, 111, 655
- Hickson P., 1982, ApJ, 255, 382
- Hickson P., Kindl E., Auman J., 1989, ApJS, 70, 687
- Hickson P., Mendes de Oliveira C., Huchra J.P., Palumbo G.G.C., 1992, ApJ 399, 353
- Hickson P., 1993, Astrophys. letters & Communications Vol. 29 numbers 1-3
- Huchtmeier W., Tammann G., 1992, A&A, 257, 455

- Laval A., Boulesteix J., Georgelin Y.P., Georgelin Y.M., Marcelin M., 1987, A&A, 175, 199
- Lequeux J., 1983, A&A, 125, 394
- Longo G., Busarello G., Lorentz H., Richter G., Zaggia S., 1994, A&A, 282, 418 (L94)
- Macchetto F., Pastoriza M., Caon N., Sparks W.B., Giavalisco M., Bender R., Capaccioli M., 1996, A&AS, 120, 463
- Mendes de Oliveira C., 1992 PhD Thesis of British Colombia University
- Mendes de Oliveira C., Plana H., Amram P., Bolte M., Boulesteix J., 1998, ApJ, in press
- Menon T.K., 1995, MNRAS 274, 845
- Mulchaey J., Zabludoff A., 1998 ApJ, 496, 73
- Oosterloo T., Iovino A., 1997, *The Second Stromlo Symposium: The Nature of Elliptical Galaxies* ASP Conf. Series Vol 116 p358. Ed M. Arnaboldi, G.S. Da Costa, P. Saha
- Osterbrock D.E., 1974, *Astrophysics of Gaseous Nebulae (W.A. Freeman and Company, San Francisco* p. 71
- Ponman T.J.; Bournier P.D.J., Ebeling H., Bohringer H., 1996, MNRAS 283, 690
- Ramella M., Diaferio A., Geller M.J., Huchra J.P., 1994, AJ 107, 1623
- Rubin V.C., Hunter D.A., Ford K.W., 1991, ApJS, 76, 153
- van Gorkom J.H., 1991, *Morphological and physical classification of galaxies* p223. Ed. Longo G., Capaccioli M., Busarello G.
- van Gorkom J.H., Schiminovich D., 1997, *The Second Stromlo Symposium: The Nature of Elliptical Galaxies* ASP Conf. Series Vol 116 p310. Ed M. Arnaboldi, G.S. Da Costa, P. Saha.
- Verdes-Montenegro L., Yun M., Perea J., del Olmo A., Ho P. 1998, ApJ 497, 89
- Zabludoff A., Mulchaey J., 1998 ApJ, 496, 39

Fig. 1.— Continuum image of H90b, c and d. The contours (in arbitrary units) were plotted after a rectangular smoothing with a box of 3×3 pixels.

Fig. 2.— (a) Monochromatic image of H90c in the $H\alpha$ line. The iso-intensities are displayed in $10^{-18} \text{ erg s}^{-1} \text{ cm}^{-2} \text{ arsec}^{-2}$ units. The lowest level is 2.4 and the step is 3.5. The position of the stellar major axis as determined from the continuum image and the position of the kinematic major axis of the gas are labeled. The cross represents the monochromatic center, which is coincident with the continuum center within a seeing disk. (b) Velocity field of the gas component. The positions of the kinematic major axis of the gas (determined in this work) and the stellar kinematic major axis (from L94) are labeled. The cross represents the gas kinematic center and the cross in bold face represents the continuum center of the galaxy.

Fig. 3.— (a) Average line-of-sight velocity curve for H90c (filled circles), at $PA=40^\circ$ (i.e., the kinematic major axis for the gas component of this galaxy). The horizontal dotted line corresponds to a central gas velocity of 2785 km s^{-1} (the kinematic center). Crosses represent all measured values within 15° of the kinematic major axis ($PA=40^\circ$). (b) VC of the gas component of H90c along a $PA=130^\circ$ (i.e., the kinematic minor axis of the gas component of this galaxy) using the continuum center. Crosses represent all measured gas velocities within 15° of $PA=130^\circ$, in order to simulate a long slit and allow a comparison with the stellar VC. Closed triangles represent the stellar VC of H90c (from L94) along a slit with the same PA. The horizontal line marks the velocity at the continuum center, 2771 km s^{-1} .

Fig. 4.— (a) Monochromatic image of H90B in the $H\alpha$ line. The iso-intensities are displayed in $10^{-18} \text{ erg s}^{-1} \text{ cm}^{-2} \text{ arsec}^{-2}$ units. The lowest level is 8.9 and the step is 4.3. Crosses represent the continuum center for H90b and H90d. The positions of the gas major axes for H90b and H90d (as measured from the $H\alpha$ images) are labeled. The stellar photometric major axis (measured from the continuum image) is almost coincident with the gas major axis. (b) Velocity field for the gas component of H90b. Crosses represent the gas kinematic centers of H90b and H90d. The crosses in bold face are the corresponding continuum centers. The kinematic major axes for the gas components are labeled for both galaxies. Also shown is the kinematic major axis for the stellar component (from L94).

Fig. 5.— Variation of the PA of the major axis as a function of distance to the center of the galaxy (Radius) for galaxies H90b and d, as measured from the geometry of their gas velocity fields.

Fig. 6.— Line-of-sight velocity curve (VC) of H90b and d. Plots have been made at $PA=60^\circ$ for H90b and at $PA=75^\circ$ for H90d (these correspond to the major axes defined by the geometry of the gas kinematics of these galaxies). The vertical long-short line represents the kinematical center of H90d (located $27''$ to the SW of H90b). The horizontal long-short line represents the systemic velocity of H90d (i.e., 2635 km s^{-1}). The vertical dotted line is the center of H90b and the horizontal dotted line is the systemic velocity of H90b (i.e., 2540 km s^{-1}). The symbols "x"

and ”+”) represent all measured values within 15° of the kinematic major axes . The filled circles are the average velocities at each radius.

Fig. 7.— (a) Monochromatic image of H90d in the $H\alpha$ line. The iso-intensities are displayed in $10^{-17} \text{ erg s}^{-1} \text{ cm}^{-2} \text{ arsec}^{-2}$ units. The lowest level is 3.0. The step is 1.2. The crosses represent the monochromatic centers of H90b and H90d. These are coincident with the positions of the continuum centers. The gas major axes for the two galaxies are labeled. The stellar photometric major axis is not shown because it is very close to the gas major axis. (b) Velocity field for the gas component of H90d. The crosses represent the gas kinematic centers of the two galaxies. The crosses in bold face represent the continuum centers. The kinematic gas major axes are labeled. Also shown is the kinematic major axis of the stellar component (from L94).

Fig. 8.— Line-of-sight velocity curves of galaxies H90b and d along a $PA=68^\circ$. The curves have been obtained by doing a cross section of the velocity maps of the galaxies at $PA=68^\circ$ and using the continuum center of H90b as a reference point (position 0,0 on this plot), in order to be consistent with L94 and allow a comparison with their Fig. 7a. The dotted horizontal line is the velocity of H90b at its continuum center (i.e., 2570 km s^{-1}) and the horizontal dashed line is the velocity at the continuum center of H90d (i.e., 2688 km s^{-1}). The dotted and dashed vertical lines represent the centers of H90b and H90d respectively. The symbols ” \times ” and ”+” represent all measured values within 15° of the axis with $PA=68^\circ$, in an attempt to mimic a long-slit at this position angle.

Fig. 9.— Profiles in the overlapping region of H90b+d. Upper panel shows the continuum map in the region between H90b and H90d. H90b is in the NE and H90d is in the SW of the map (north is up and east is to the left). The bold face square represents the area where the profiles have been extracted. The lower left panel shows the data. Each square represent a pixel, or $0.91''$ on the sky, and an interval of 380 km s^{-1} in velocity space. The lower right panel shows a gaussian fit to the profiles (FWHM of 63 km s^{-1}).

Fig. 10.— The ratio of the ionized gas mass to K band luminosity as a function of radius for H90b, H90c and H90d. The absolute scale for the K photometry is not accurate but the relative differences in the shapes and intensities of these curves are not affected by this uncertainty.

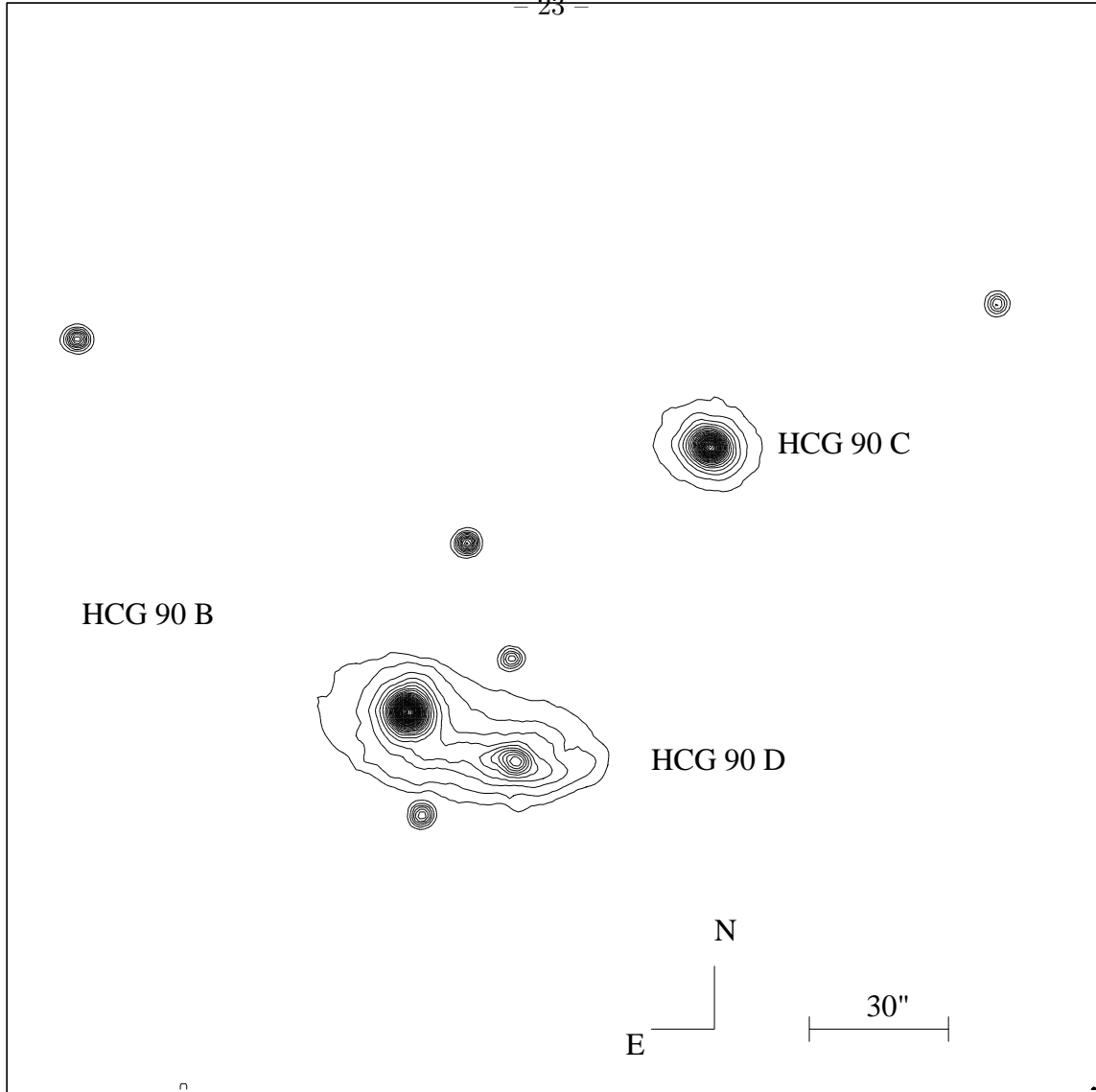


Fig. 1

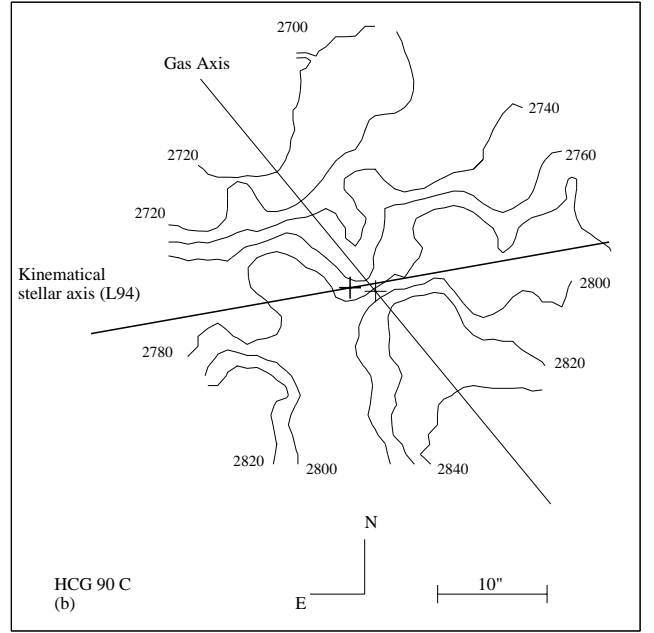
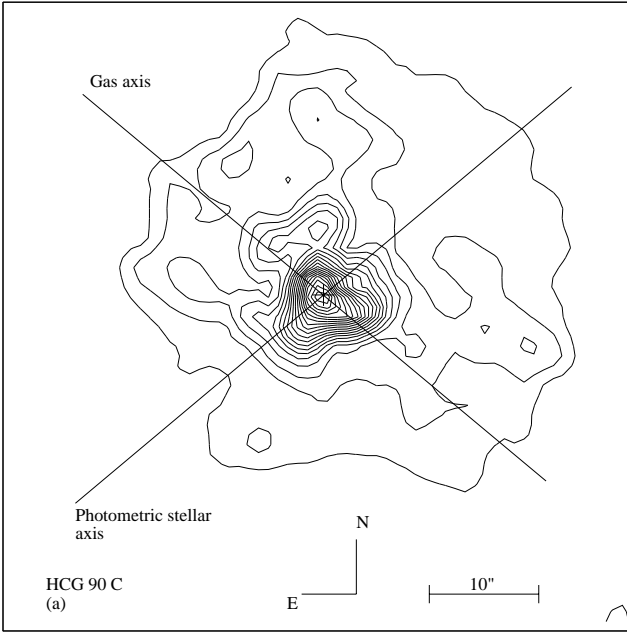


Fig. 2

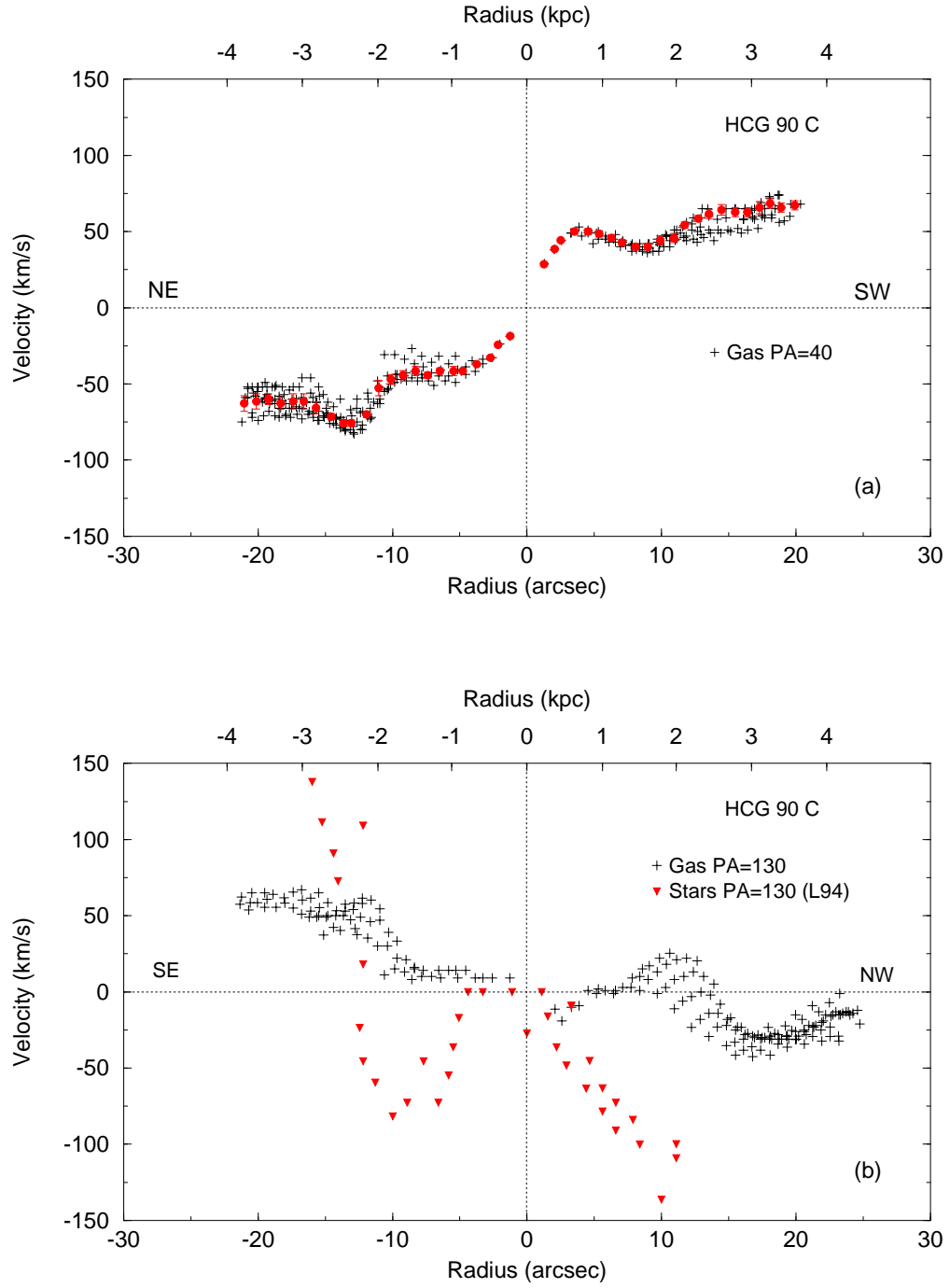


Fig. 3

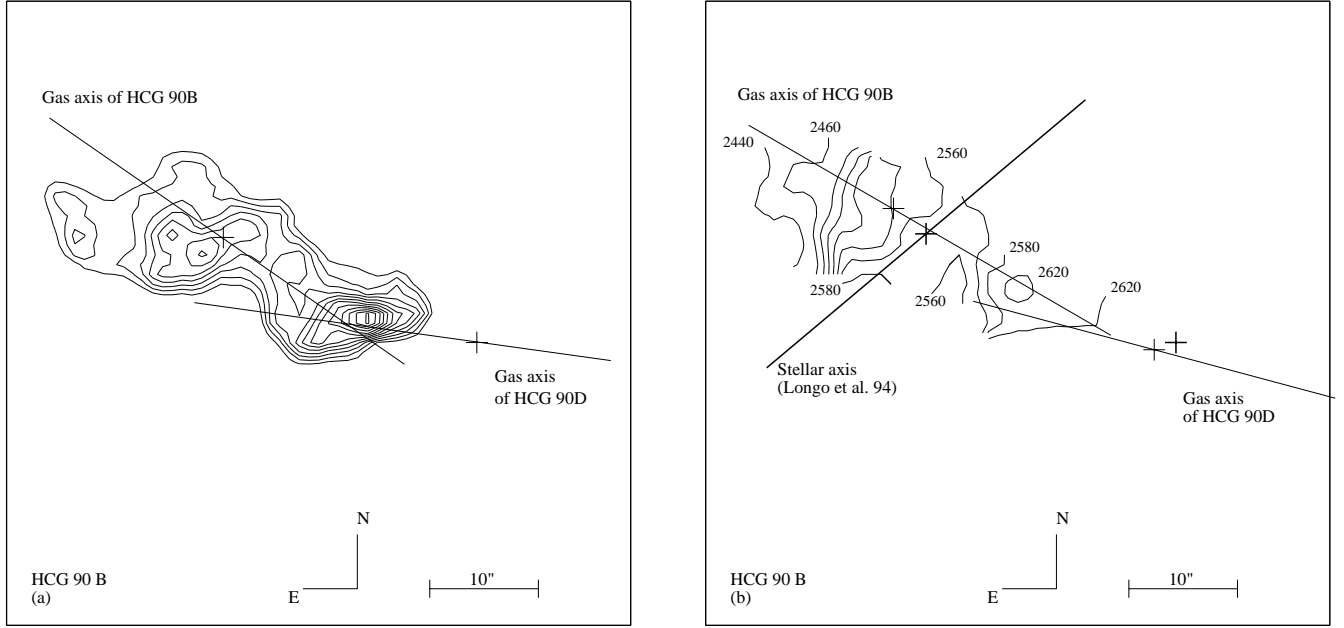


Fig. 4

Fig. 5

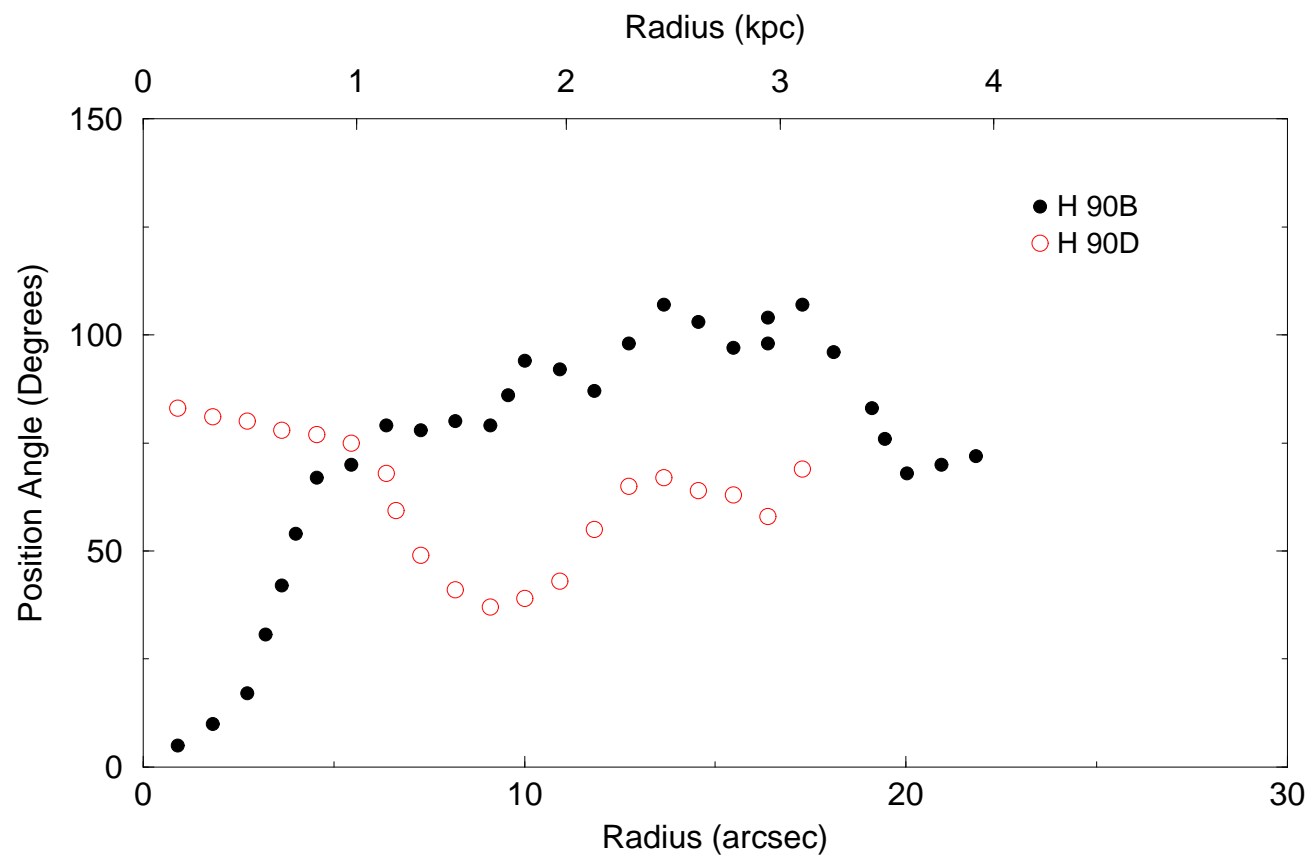
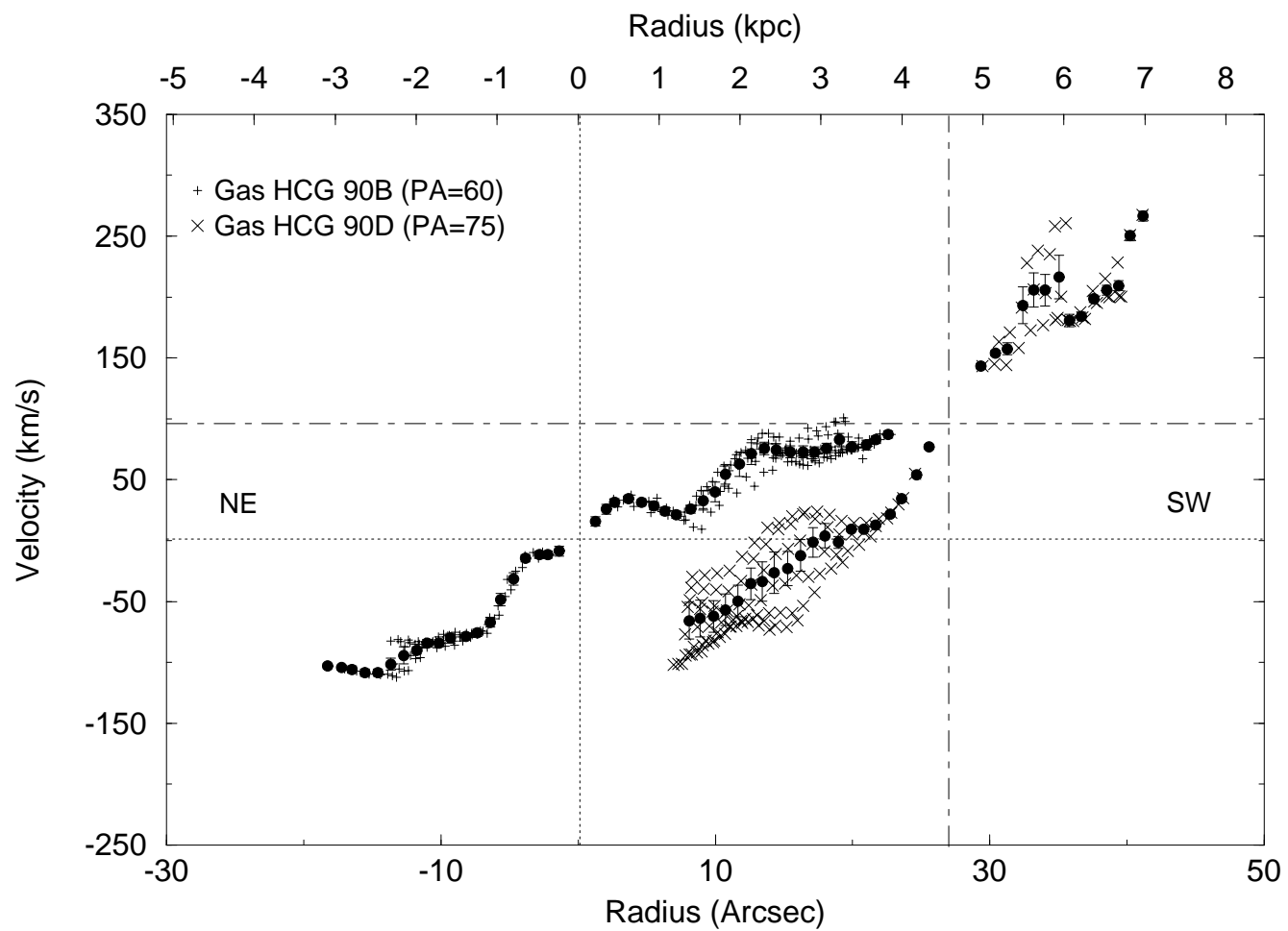


Fig. 6



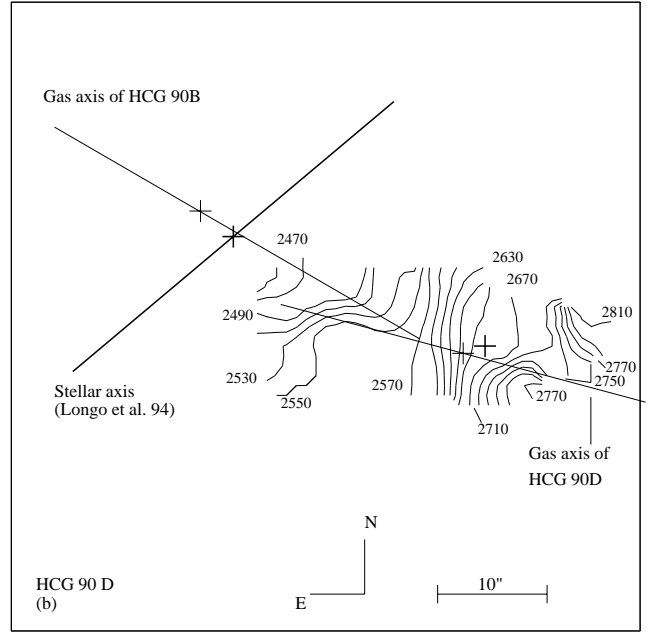
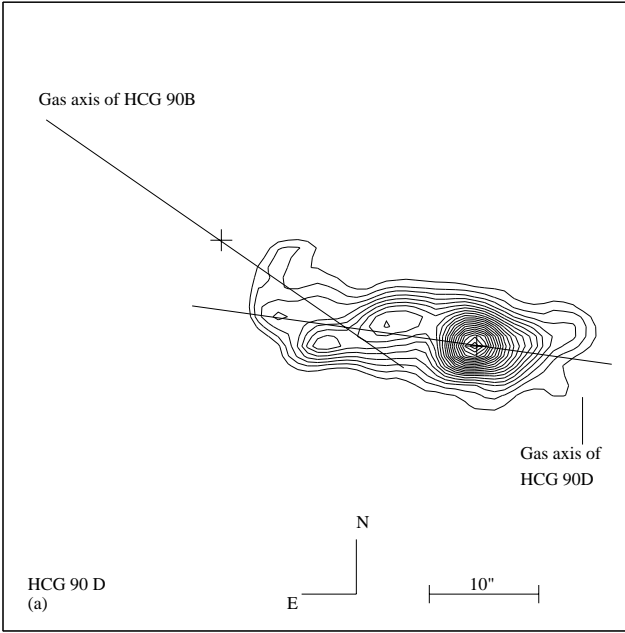
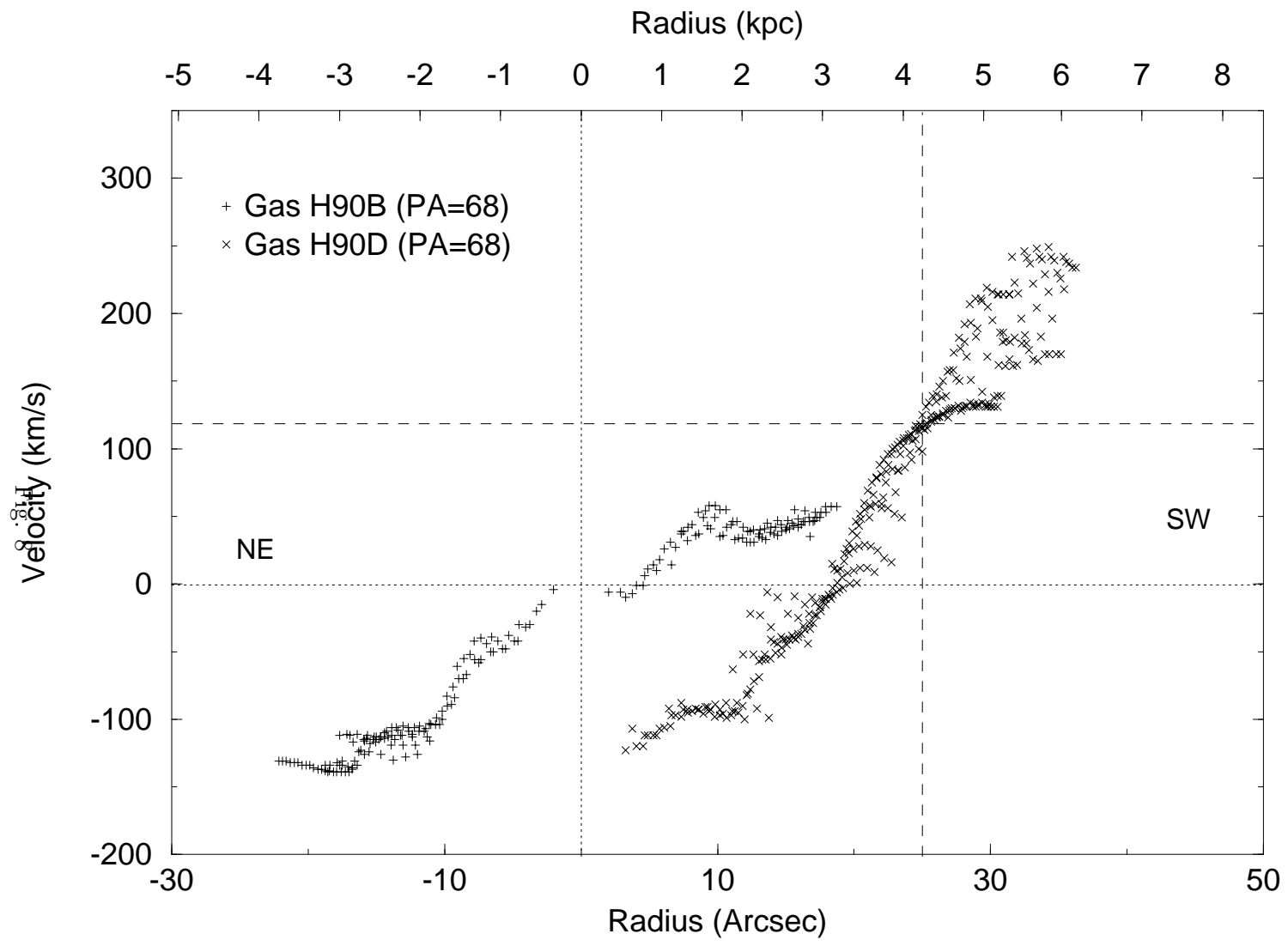


Fig. 7



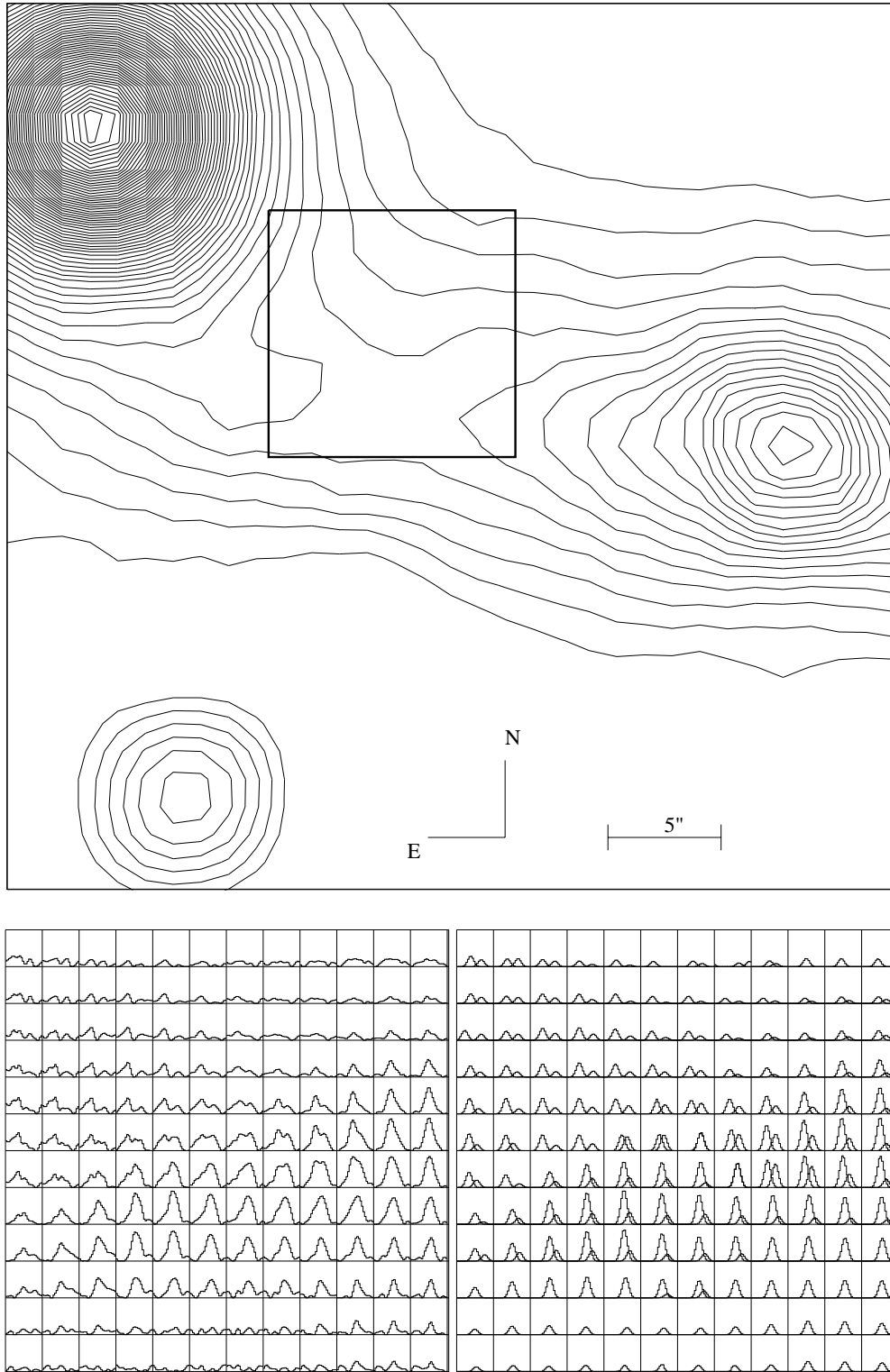


Fig. 9

Fig. 10

